Laminar flow and heat transfer in triply periodic minimal surfaces

André Gonçalves Pereira Passos
andre.passos@tecnico.ulisboa.pt

Instituto Superior Técnico, Universidade de Lisboa, Lisboa, Portugal

July 2019

Abstract

Metallic open-cell foams have desirable properties such as high porosity, specific area and tortuosity. These features are suitable for the improvement of heat exchanger performance as it allows higher heat transfer rates for the same volume when compared with traditional geometries. With the development of additive manufacturing the opportunity to tune porous media geometry has emerged and it is now possible to use complex topologies as triply periodic minimal surfaces. Triply Periodic Minimal Surfaces are mathematically defined surfaces, infinite in 3-D space, that minimize local mean surface curvature for a given boundary and can divide space in two continuous regions intertwined with one another with smooth curvatures and no edges or angles rendering them suitable candidates to newly engineered porous media to enhance heat transfer while minimizing pressure drop. To evaluate its properties detailed solutions of the Navier-Stokes equations were obtained for periodic 3-D cells based on the Schwarz-P, Schwarz-D and Schoen Gyroid topologies with different wall thicknesses. The inertial regime was described, and transition Reynolds numbers were obtained. Pressure drop was calculated using Darcy-Forcheimmer law and friction factor. To assess heat transfer capabilities effective thermal conductivities and constant wall temperature Nusselt numbers were obtained. Finally heat transfer, pumping power and material use efficiency were compared with the benchmark case of the flat plate.
Keywords: porous media, triply periodic minimal surfaces, laminar flow, convective heat transfer, heat exchangers

1. Introduction

Heat exchangers have a crucial role on the efficiency of numerous applications such as automotive and aerospatial industries, food and chemical industries, power production, manufacturing industries and air quality equipment to name a few and nowadays increase in performance of the equipment is crucial. In the later years thermal improvement has been investigated based on the use of extended surfaces, that includes porous media, to increase the surface-to-volume ratio, at the expense of increased pressure drop and in heat exchangers the use of metal foams has been investigated due to structural strength allied high thermal conductivity. Understanding all the phenomena of fluid flow and heat transfer in porous media is a difficult task due to the geometric complexity and random orientation of the solid phase. This difficulty in analytical and computational studies has been tackled with the analysis of idealized geometries [12, 11] and volume averaged equations over a representative elementary volume although in the laminar regime it is enough to define volume averaged characteristics such as porosity, permeability and form drag coefficient to describe the fluid flow based on Darcy-Forchheimer law. Regarding the heat transfer two approaches are available depending on the problem in hands. When the local temperature differences between solid and the fluid phases are negligible the thermal properties can be averaged over both domains, and therefore results in a single energy equation and an effective thermal conductivity (k_{eff}) is defined accounting for both phases. Mendes et al. [12] investigated various methods for prediction of k_{eff} and concluded that when the ratio between the conductivities of the fluid and the solid domains are very small k_{eff} can be approximated by k_{eff} of the solid phase only. When the local temperature differences between phases are significantly different there is the need of a two energy equations model, for the solid and the fluid domains separately and it is necessary to define of convection heat transfer coefficients [16].

Triply Periodic Minimal Surfaces (TPMS) are mathematically defined surfaces, infinite in 3-D space that minimize local mean surface curvature for a given boundary [14, 1]. This kind of surfaces can divide space in two continuous regions intertwined with one another with smooth curvatures and no edges or angles [8]. While minimising sur-

face area, TPMS present the opportunity to create new lightweight yet stiff structures for several applications [1], and several authors have investigated their properties. Abbueida et al.[2] investigated mechanical properties of TPMS experimentally and numerically and also made finite-element simulations to obtain electrical/thermal effective conductivities of several TPMS, including the ones studied in this work, for several wall thicknesses and compared with plate, fibres and particle reinforced composites. Guest and Prévost [6] made an optimization study that achieved a surface similar to Schwarz-P surface with an algorithm to maximize permeability of microstructures. Femmer et al. [5] created several micro heat exchangers with four different TPMS working in cross-flow and analysed the thermal performance in low Reynolds regime (up to $Re = 12$) and reported promising results as far as heat transfer and effectiveness, although pressure drop across the heat exchanger was predicted using numerical simulation.

The goals of this work is the evaluation and comparison of metal foams properties (permeabilities, form-drag coefficients, k_{eff}, Nusselt numbers, friction factors and effectivenesses) based on the Schwarz-P (SP), Schwarz-D (SD) and Schoen-Gyroid (G) topologies with different wall thicknesses by means of detailed solutions of the 3-D Navier-Stokes equations in 3-D periodic cells using the Star-CCM+® code.

2. Background

2.1. Volume averaged governing equations

At microscopic scale the continuity, momentum transport and energy equations can be used if a representative number of pores are considered, and hence, macroscopic information can be post-processed for a Representative Elementary Volume (REV) [15]. Considering a saturated porous medium with a single fluid phase the application of the Volume-Average theorem to the Navier-Stokes equations results in the equations [15]:

$$\nabla \cdot \langle \vec{v} \rangle = 0 \tag{1}$$

$$\rho \frac{\partial \langle \vec{v} \rangle}{\partial t} + \rho \langle \vec{v} \rangle^f \nabla \cdot \langle \vec{v} \rangle^f + \frac{\rho}{\phi} \nabla (\langle \vec{v}\, \hat{v} \rangle) = - \nabla (\langle p \rangle^f) + \mu \nabla^2 \langle \vec{v} \rangle^f + \rho \vec{g} + \frac{1}{V_T} \int_{A_{sf}} (-\hat{p} + \mu \nabla \vec{v}) \cdot \vec{n} \, dA \tag{2}$$

From the work of Kuwahara et al. [10], there are 2 models for volume-averaged energy equations. If the flow regime is under low Péclet numbers ($Pe = RePr$), we can assume local thermal equilibrium, $\langle T \rangle^f = \langle T \rangle^s = \langle T \rangle$, and therefore is possible to combine the fluid and solid equations into a single equation that treats the two phases as a single medium [9]:

$$(\rho C)_{eff} \frac{\partial T}{\partial t} + \rho_f C_p \langle \vec{v} \rangle \cdot \nabla T = \nabla \cdot (k_{eff} \nabla T) \tag{3}$$

where $(\rho C)_{eff}$ is the effective heat capacity of the solid and fluid phases combined. According to Mendes et al. [12] for low k_f, k_{eff} can be approximated by the effective thermal conductivity of the solid phase only, $k_{eff,s}$. Taking a cubic unit cell with side L_r, k_{eff} is given by:

$$q'' = k_{eff} \frac{T_H - T_C}{L_r} \tag{4}$$

where q'' is the average steady-state heat flux in x_1 direction. A temperature difference of $T_H - T_C$, with $T_H > T_C$, is applied in the x_1 direction and the remaining four boundaries are considered adiabatic. If the hypothesis of local thermal equilibrium breaks down, two equations are needed to account for energy in the solid and fluid phases. This two-equations model has been presented in the literature has it follows [10]:

$$\phi \rho_f C_p \left[\frac{\partial \langle T \rangle^f}{\partial t} + \langle \vec{v} \rangle^f \cdot \nabla \langle T \rangle^f \right] = \nabla \cdot (\overline{k}_{eff,f} \cdot \nabla \langle T \rangle^f) + h_{sf} \, a_{sf} (\langle T \rangle^s - \langle T \rangle^f) \tag{5}$$

$$(1 - \phi) \rho_s C \frac{\partial \langle T \rangle^s}{\partial t} = \nabla \cdot (\overline{k}_{eff,s} \cdot \nabla \langle T \rangle^s) - h_{sf} \, a_{sf} (\langle T \rangle^s - \langle T \rangle^f) \tag{6}$$

where $\overline{k}_{eff,f}$ and $\overline{k}_{eff,s}$ are the effective thermal conductivities tensors of the fluid and solid phase respectively, $a_{sf} = A_{sf}/V$ is the specific surface area, and h_{sf} is the interfacial convective heat transfer coefficient. $\overline{k}_{eff,f}$, $\overline{k}_{eff,s}$ and h_{sf} have to be determined.

2.2. Empirical flow model

For internal flows the Reynolds number is based on the mean tube velocity and the diameter or hydraulic diameter but for porous media there is no consensus among authors on either the velocity used or the characteristic length and this makes it difficult to choose a Re to compare and validate results. Following the work of several authors [15, 3] the characteristic length used on this work is th hydraulic diameter defined by:

$$d_h = \frac{4 \, \phi}{a_{sf}} \tag{7}$$

where ϕ is the porosity. The Reynolds number is defined by:

$$Re = \frac{\rho \ v_p \ d_h}{\mu} \tag{8}$$

where v_p is the pore velocity and is related to the Darcian velocity by $v_d = \phi \ v_p$. The flow through porous media can be divided in four distinct flow regimes [3]:

- $Re <$ 1, Darcy or creeping regime - laminar steady
- 1–10 $< Re <$ 150, moderate Forchheimer (or inertial) regime - laminar steady
- 150 $< Re <$ 300, strong Forchheimer (or inertial) regime - Laminar unsteady
- $Re >$ 300, Turbulent

The scope of this work lays in the inertial regime where the effects of inertia and form-drag are considered and the pressure drop is related to the superficial velocity with the Darcy-Forchheimer law.

$$\frac{\Delta p}{L} = -\frac{\mu}{K} \ v_d - \frac{\rho \ c_f}{\sqrt{K}} \ v_d^2 \tag{9}$$

2.3. Heat transfer in internal flows

In internal flow it is usual to define pressure drop in the dimensionless form given by the Darcy friction factor (f) defined by:

$$f = \frac{\Delta P}{\frac{1}{2} \ \rho \ v_p^2 \ \frac{L}{d_h}} \tag{10}$$

Regarding the thermal boundary condition at the wall, according to Shah and London [13] if the wall conductivity k_s in the axial and peripheral directions are high enough to be considered infinite, in the radial direction k_s can be an arbitrary value that the proper boundary condition to use is constant temperature. To characterise heat transfer across the wall it is needed the convection heat transfer coefficient (h) and its dimensionless form the Nusselt number (Nu). For convection heat transfer definition, h is given by:

$$h = \frac{q''}{\Delta T_{LM}} \tag{11}$$

where ΔT_{LM} is the mean-log temperature difference. This definition although it does not enter directly in volume-averaged energy equations, it allows the comparison of h of porous media with other internal flows as the case of the flat-plate and this is the definition used in this work. With the definition of h established, Nu is defined by:

$$Nu_x = \frac{h \ x}{k_f} \tag{12}$$

where x are the characteristic lengths use in this work the hydraulic diameter d_h or the periodic length L. The effectiveness (ϵ) relates the actual heat transfer rate for a heat exchanger to the maximum possible heat transfer rate accounting only for convection. This is defined as:

$$\epsilon \equiv \frac{T_{in} - T_{out}}{T_{in} - T_s} \tag{13}$$

For high enough Pe numbers it is a valid approximation but for $Pe < 30$ this assumption no longer holds due to the axial conduction mechanism along the fluid domain, not taken into account.

3. Implementation

3.1. Surface creation

The geometry creation starts with the generation of TPMS using the software *Surface Evolver* to obtain stl files. Afterwards the surfaces are transferred to the software Solidworks® to be thickened and create the fluid counterparts. Finally the wall and fluid domains are transferred to the CFD software Star-CCM+® for simulation.

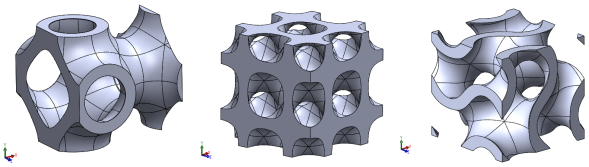

(a) (b) (c)

Figure 1: TPMS analysed in this work: SP (a), SD (b) and G (c).

3.2. Numerical model

After the domain is imported into Star-CCM+® a finite volume mesh is built with polyhedral cells and prism layers in the fluid solid interface. For the physical models, for both the fluid and solid domains the following assumptions were made: steady state incompressible flow with constant properties and heat transfer. All the simulations were made with $\rho = 1 \ kg/m^3$, $\mu = 2 \times 10^{-5} Pa \cdot s$ and $k = 0.01 \ W/m \ K$ as fluid properties and $C = 903 \ J/kg \ K$ and $k = 237 \ W/m \ K$ as solid properties. For boundary conditions fully developed flow interfaces normal to the x direction were with prescribed bulk temperatures of $T_{h,in} = 363 \ K$ in the hot channel and $T_{c,in} = 293 \ K$ in the cold channel, and periodic pairs of internal interfaces in the boundaries normal to the y and z directions. The solid walls have no-slip condition at the fluid-solid interfaces, are adiabatic in the boundaries normal to the x-direction and have periodic interfaces in the boundaries normal to the y and z directions. The convergence criteria was set at a value of 10^{-7} for all the residuals as negligible variations in the measured quantities were verified.

3.3. Verification and validation

In the verification process a grid independence study was executed on a REV of a unit cubic cell, 12mm x 12mm x 12mm, composed of a solid domain modelled after the G surface and two fluid domains. The cell was designed to have 70% total porosity and constant wall thickness of 1.2mm. For grid convergence evaluation it was calculated f and Nu_{d_h} were calculated at $Re = 25$ for 8 different meshes. From Figures 2(a) and (b) it can be inferred that there are no significant differences between the last two meshes in terms of pressure loss and heat transfer. In fact from mesh 7 to mesh 8 there is only difference of 0.26% in terms of the averaged Nu_{d_h} of the two channels and -0.05% for the friction factors averaged between the two channels. Comparing the results for each channel independently, the difference between them is of 0.03% for the Nu and 0.01% for the friction factor.

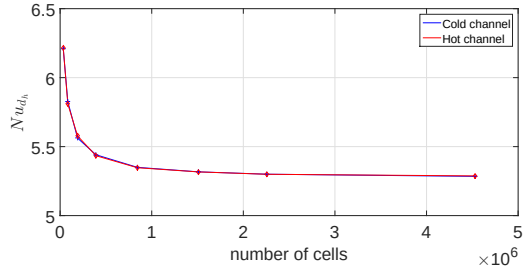

(a)

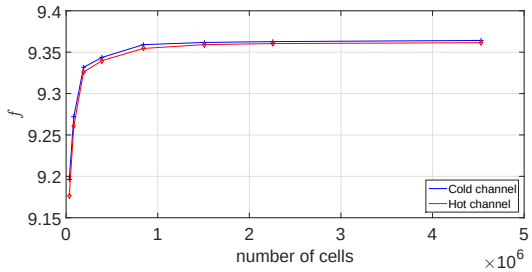

(b)

Figure 2: Results of grid convergence for $Re = 25$: Nu_{d_h} (top) and f (bottom).

For the code validation, 2D simulations of a flat plate heat exchanger were performed. On the top and bottom walls periodic boundary conditions were used, the flow was made fully developed to obtain the fully developed pressure drop along the channel and heat flux through the walls. The walls boundaries normal to the x-direction were assumed adiabatic.

In the Figure 3 (b) it is shown the evolution of f with Re in one of the channels and the curve fits perfectly with the theoretical curve described by $f = 96/Re$ with the difference between the simulations and the theoretical curve being of 0.03% on all

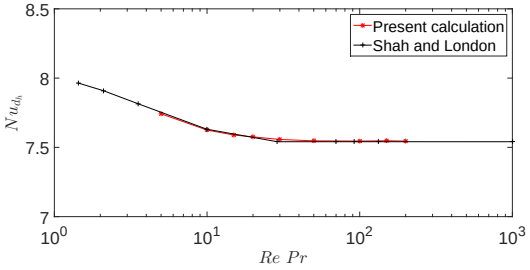

(a)

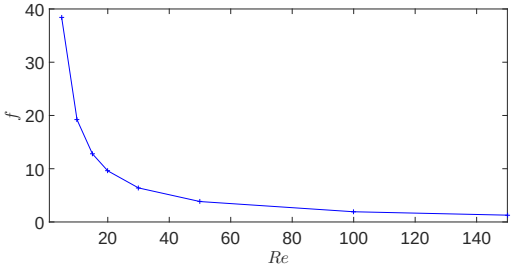

(b)

Figure 3: Results of grid convergence for $Re = 25$: Nu_{d_h} (a) and f (b).

points. With respect with Nu_{d_h} the results of the simulations compare very well with the theoretical values referred by Shah and London [13] with Nu_{d_h} tending towards the constant value of 7.54 for large Pe, as it should for the constant wall temperature case and for $Pe < 50$ the effects of axial conduction along the fluid become more pronounced and the effect on Nu_{d_h} is notorious by its increase with lower Pe.

4. Results

An example of domains used can be seen in Figure 4. After a first post-processing of the results, it was chosen to evaluate the effect of wall thickness on SD and G surfaces and it was created the SDt and Gt cases with $t/L = 1/30$. In Table 1 it can be found the relevant geometric features of each case. It is noted that due to the complementary nature of TPMS, ϕ_c and ϕ_h corresponds to the porosity of cold or hot channels respectively and $\phi_c + \phi_h = \phi$. The wall volume V_s it is also listed in Table 2 as a reference of the material used in manufacturing. In the first four geometries analysed the same wall thickness was used, given by the parameter t/L, but due to topology differences, different values of ϕ are obtained for each surfaces.

4.1. Effective thermal conductivity

Considering only the solid domains, k_{eff} was calculated for the three topologies using the equation (4). The results are resumed in Figure 5 where it is plotted the evolution of k_{eff}/k_s with ϕ. The plot also presents the results of SP and SD surfaces cal-

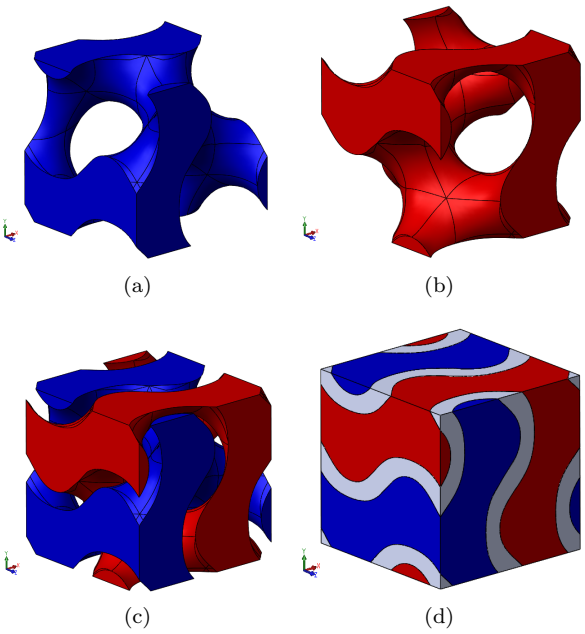

Figure 4: Geometric domains of G unit cell: Unit cells of cold fluid channel (a), unit cell of hot fluid channel (b), unit cells of intertwined fluid domain (c) and the full REV(d).

Table 1: Geometric properties of the topologies analysed.

Type	t/L	$\phi_{c,h}$	ϕ	$(a_{sf})_{c,h}$ $[m^{-1}]$	a_{sf} $[m^{-1}]$	$(d_h)_{c,h}$ $[mm]$
Flat plates	1/10	0.4	0.8	166.667	333.333	9.60
SP	1/10	0.384	0.768	190.138	380.275	8.08
SD	1/10	0.312	0.624	300.189	600.378	4.16
G	1/10	0.349	0.698	247.972	495.943	5.63
SDt	1/30	0.436	0.872	318.487	636.973	5.48
Gt	1/30	0.449	0.898	256.944	513.889	6.99

Table 2: Material volume used at the wall.

Geometries	V_s $[\times 10^{-7}\ m^3]$
Flat plates	3.456
SP	4.015
SD	6.499
G	5.219
SDt	2.209
Gt	1.768

culated by Abueidda et al. [2], with proper scaling, and the results of anisotropic foams calculated by Mendes et al. [12]. As seen in Figure 5 the SP and G surfaces have the highest values of k_{eff}/ks with both curves being almost coincident. This is validated when comparing the curves of SP and G obtained in this work with the results of Abueidda et al. [2]. The results of k_{eff}/k_s for the SD surface are 10% lower than SP and G but significantly different from the results of Abueidda et al. [2]. In their work, it was reported low connectivity at the boundary of the unit cell as the cause of low values and this may be due to the use of the surface inserted in rhombic dodecahedron unit cell rather than in a cubic unit cell. Comparing the results with the calculations for anisotropic foams made by Mendes et al. [12] it can be seen that, for the same porosity, TPMS present far superior performance.

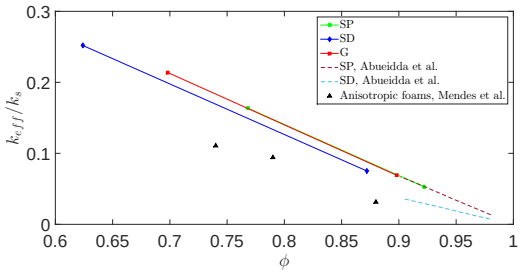

Figure 5: Effective thermal conductivities.

4.2. Flow Analysis

The flow through the SP topology is dominated by two main features: the contraction area and the recirculation bubbles, as seen in Figure 6. The contraction area creates preferred flow lanes, as the flow across aligned tube banks referenced by Incropera et al. [7], and the rest of the volume remains at wake of the wall as it can be seen on Figure 6. Due to this flow arrangement, the surface is not used to the full extent and the effective contact between the fluid and the wall changes with the size of the recirculation zones. The size of the recirculation zones increase from $Re = 5-25$ and remain constant until the transition. After $Re = 75$ the flow begins to oscillate and transits to the laminar unsteady regime.

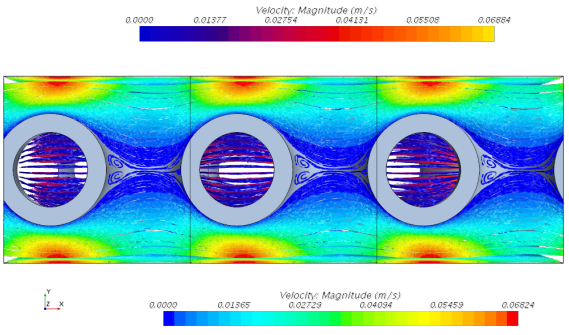

Figure 6: SP streamlines across three REVs for Re=5.

The SD surfaces create structures similar to a diamond cubic crystalline with its voids that allows

five connection points per unit cell in each channel were the flow can mix. Until $Re = 45 - 60$, the flow in this mixing regime follows perfectly the arrangement described above and, due to the mixing in the connection points, the flow creates homogeneous temperature field. Between $Re = 50 - 60$ and up to $Re = 75 - 100$, due to inertia, the flow starts to deviate from the crystalline structure and creates preferred flow lanes, as in the SP surface, that lower the increase in heat exchanged. This transitional laminar regime depends on the wall thickness, where thick walls push the transition regime towards lower Re, and thinner walls have the transitional regime at higher Re. This is verified by the wall thickness study made where for $t/L = 1/10$ the transitional regime is between $Re = 50 - 75$ and for $t/L = 1/10$ it stands at $Re = 60 - 100$. After the transitional regime, the flow is completely differentiated and in each channel it is possible to see distinct flow lanes with very little mixing between the two. This evolution is represented by Figure 7. Heat transfer, although continues to increase, it does so but at a lower pace as comparing with the mixing regime. For either thick or thin versions of the surface transition to laminar unsteady regime occurs at $Re = 150$.

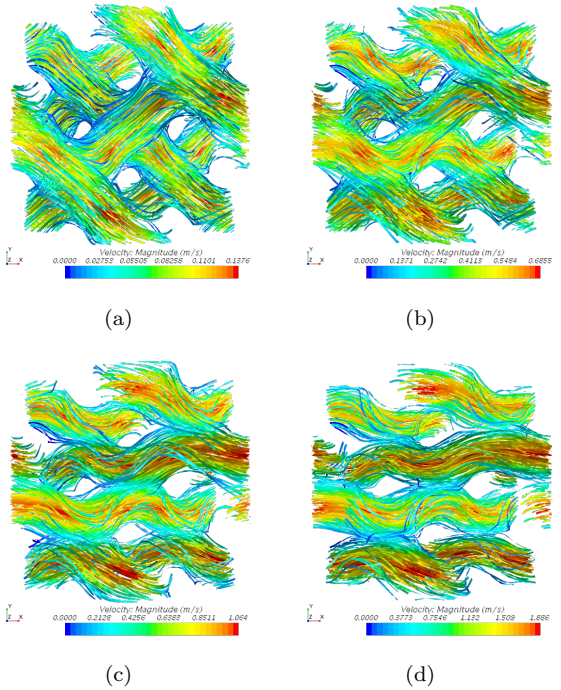

(a) (b) (c) (d)

Figure 7: SD streamlines for Re=10 (a), Re=50 (b), Re=75 (c) and Re=125 (d) seen perpendicularly to the axial direction from left to right.

The flow through G surfaces is divided in two streams on each channel twisted along the axial direction. In Figures 8 (a) and (b) it is possible to see the evolution of tangential velocity with increasing Re. The flow maintains the structure with increasing Re up to $Re = 75$ where the abrupt change in direction seen at the interfaces between the two streams and the wall give way to vortices as in Figure 8(b). After $Re = 75$ the flow becomes unsteady.

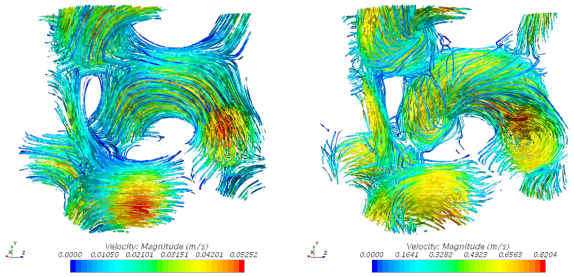

(a) (b)

Figure 8: G streamlines at the cold channel for Re=5 (a) and Re=75 (b).

4.3. Pressure Drop

In order to use a simplified porous media models in CFD, the results of pressure drop from the simulations were fitted to Darcy-Forchheimer law with the least square method, and the values for permeability and form-drag coefficient present on Table 3 and Figure 9 were obtained. Table 3 shows that SP surface, due to low contact with the wall, has the highest permeability and the lowest form-drag of the three surfaces analysed, with the same wall thickness. This is in agreement with the results of Guest and Prévost [6] although their results were obtained only for the creeping flow regime. Comparing the coefficients of G and SD surfaces, one can see that the permeability of SD is almost half of that for G and although the form drag of G is higher than that of SD, the latter surface has higher pressure gradients as seen in Figure 9.

Table 3: Permeability and form-drag coefficients for TPMS.

Geometry	t/L	K [$\times 10^{-8}$ m^2]	c_f
SP	1/10	18.98	0.175
SD	1/10	6.55	0.599
G	1/10	12.88	0.714
SDt	1/30	13.66	0.244
Gt	1/30	23.42	0.409

Comparing the pressure gradients of SD and G surfaces with the respective thinner counterparts (SDt and Gt), the thinner versions of the surfaces have more linear pressure gradients due to the lower tortuosity induced by the wall and higher hydraulic diameters. These correlations tend to deviate from the numerical results at lower Re. For SP surface

the correlation overestimates pressure gradient by 13% at $Re = 5$ and for SD where the underestimations reach 7.6% at $Re = 7.5$. These deviations occur for all surfaces at $Re \leq 10$, but gradually decrease with increasing Re, probably due to the use of a correlation made for predictions in the inertial laminar regime.

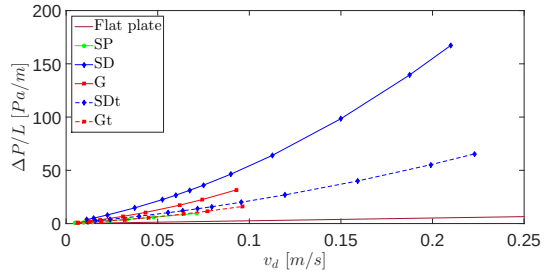

Figure 9: Plot of the Darcy-Forchheimer law fit.

In plot of friction factor of Figure 10 it is possible to see that all of the surfaces present exponential decrease of f with Re, with the flat plate having much lower values of f due to the tortuosity present in TPMS. The curve corresponding to SP surfaces gives the highest values of f for a given Re due to the dependency on d_h/v_p^2 factor. SP surface has the lowest velocities and the highest d_h of the TPMS analysed and this results in a distortion of the results. The SD and G curves are almost perfectly overlapped with the thinner versions of the surfaces meaning that the friction factor is a good parameter of pressure drop evaluation for the TPMS as the curve for a given topology is not affected too much by the wall thickness. Evaluating the friction factor, the flat plate has the advantage of maintaining the laminar regime up to $Re \approx 2000$ where the pressure drop is lower, while the steady laminar regime of TPMS has a short extension ending at $Re = 75$ to SP and G topologies and at $Re = 150$ for SD topology and afterwards transition to regimes where the pressure drop are higher due to turbulence.

Nevertheless, in the inertial steady regime, the SP topology showed the lowest values of pressure drop for the analysed TPMS, although it presented higher than the reference case.

4.4. Thermal Performance

For evaluation of the heat transfer between fluids and solids the first parameter of analysis is the Nu number, that depends on a characteristic length. As it is usual for internal flows it was calculated the Nu_{d_h} as first approach .

The values of Nu_{d_h} for SP surface present a decrease from $Re = 5 - 25$ due to two factors: the decrease in axial conduction contribution to the overall heat transferred across the wall and, as mentioned in section 4.2, the reduction of effective contact area between the preferred stream and the wall. From $Re = 25$ until the beginning of the unsteady regime, due to stabilization of the recirculation zones, the contact area remains constant and with increase of Re it is seen a slight increase of the Nu_{d_h}. Over G and Gt surfaces there is a decrease in Nu_{d_h} from $Re = 5$ to $Re = 10$ due to decrease in the fluid axial conduction contribution to the overall heat transferred. This effect is not present in SD and SDt surfaces due to the high degree of mixing that exists at low Re. After $Re = 50 - 60$ starts the transitional laminar regime with the decrease in values of Nu_{d_h} seen in the plot of Figure 11. After the change in flow structures is complete, Nu_{d_h} increases again due to the increase in mass flow. From the values of Nu plotted in Figure 11 the improvement of TPMS is not as great as expected when compared with the flat plate. Because of the higher hydraulic diameter of the flat plate and the effect of lower ϕ on d_h calculation for SD and G, the results get distorted. Using the same characteristic length for all of the topologies analysed, as the periodic length L, the results reflect better the convection properties of TPMS compared with the flat plate.

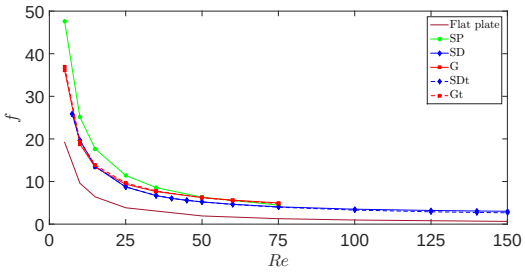

Figure 10: Friction factor vs. Re.

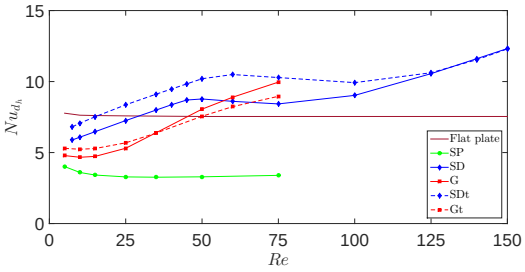

Figure 11: Nu_{d_h} vs. Re.

From the plot in Figure 12, the improvement in convection of TPMS is notorious. The values of Nu_L of the SP surfaces are not as low as compared with the flat plate, and for increasing Re, the G and Gt surfaces have greater performance in almost all of the laminar regime. SD and SD surfaces clearly outshine the flat plate in terms of convection in the laminar regime. This definition of Nu is inline with

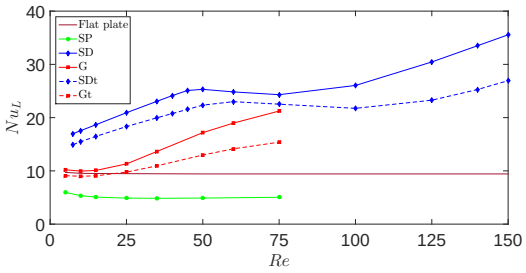

Figure 12: Nu_L vs. Re.

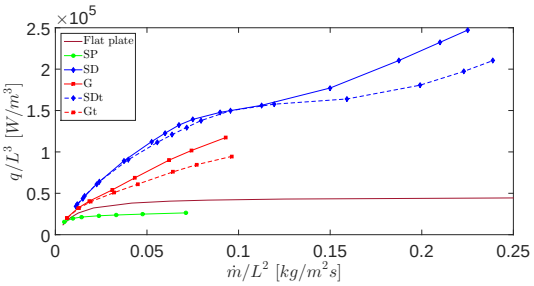

Figure 14: q/L^3 vs. mass flux.

the evolution of h with Re seen in Figure 13.

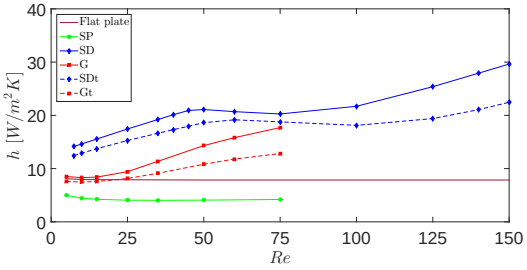

Figure 13: h vs. Re.

The change in characteristic length shows that the TPMS have superior convection properties in the full extent of the laminar regime. This means that, with transition to the unsteady laminar and turbulent regimes, the increase in convection properties of the TPMS will be even larger when compared with the flat plate that holds the laminar regime up to $Re \approx 2000$ where the convection coefficient is constant.

On Figure 14 the energy density exchanged across the REV is shown. For the SP surface, the energy density is fairly constant as expected from the Nu numbers plotted above and the same can be said about the flat plate. G and Gt surfaces have greater heat exchanged, with Gt reaching more than double than the flat plate for the maximum mass flux across Gt and G surface reaching almost triple than the flat plate for the maximum mass flux across G. SD and SDt have closely the same energy density up to the end of the mixing regime, and thereafter SD energy density increases more than SDt due to higher velocities.

To evaluate the energy traded with respect to the material used to manufacture the structure, it was plotted in Figure 15 the heat exchanged per unit of solid material to better evaluate the use of wall material and see if the use of material is as useful as it should be. From Figure 15 it is possible to see that for very low mass fluxes the flat plate is the better alternative. Until the end of the mixing regime of the SD surface, the material used in it gives the same energy output as the G surface, with the latter using less material. The thinner versions SDt and Gt stand out of the rest because of the obvious advantage of lower wall thickness. Comparing one another, SDt, even though it has more material, it surpasses Gt across all the laminar regime. The plot also suggests that, with increasing wall thickness, the G topology may be more useful than the SD topology as it gives better use for the material.

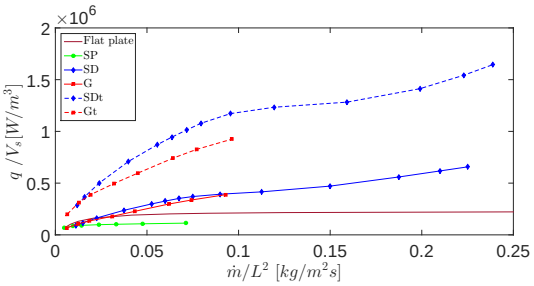

Figure 15: q/vol_s vs. mass flux.

To evaluate the efficiency of heat transfer across the wall, the ϵ was calculated and plotted on Figure 16. The SD and SDt surfaces have the best ϵ in the laminar regime, especially for $Re < 50$, and thereafter ϵ approximates to the ones of G and Gt. The wall thickness decreases the ϵ of the surface due to higher porosities. All of the TPMS analysed have superior ϵ compared to the flat plates except for SP due to the reduced contact area between the main flow and the wall. ϵ of flat plates comes near to the values of G and Gt surfaces only for $Re < 25$, although this region has some modelling errors due to the contribution of the axial conduction in the fluid domains that are not taken into account.

After evaluating the pressure drop across the TPMS and heat exchanged in the TPMS, the final thought is to compare the energy trade-off between the heat exchanged (what one gets) and the pump power required to move the fluid across (what one pays). From the results plotted in Figure 17 what stands out is the higher energy trade-off of the flat plate. In fact, due to the absence of wall blockage effect, the pump power required in flat plates

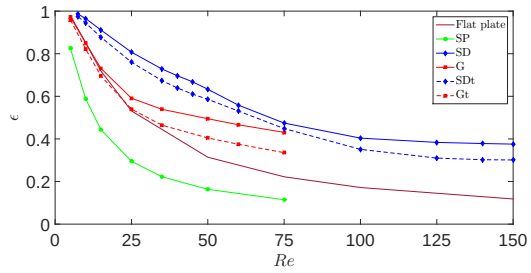

Figure 16: ϵ vs. Re.

is lower compared with the TPMS and greatly influences the results. In an overall analysis of the plot, TPMS have similar energy trade-off's, with SD having the lowest values. SP surface has the better trade-off of the TPMS for $t/L = 1/10$ at low Re, and near the transition the values are near those of G surface. The higher effective contact wall for low Re indicates that this surface is better for this regime. G topology either in thick or thin wall version has better trade-off's when compared with the SD topology. As expected, the decrease in wall thickness improves the energy trade-off as increases wall surface while decreasing pressure drop.

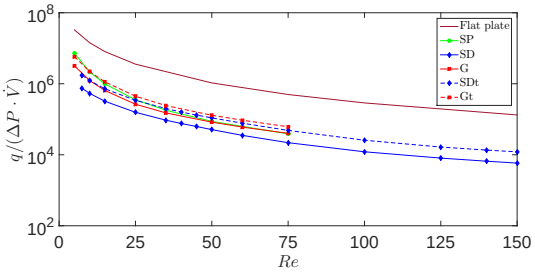

Figure 17: Energy Trade-off vs. Re.

To better summarize the results in terms of thermal performance, the TPMS are the best solution when lower space or material is needed. The SD topology, having higher Nu, allows for greater heat transfer and thermal effectiveness compared with the other surfaces in the scope of this work. Note that this conclusion is in line with the work of Femmer et al. [5]. This improvement however is made at the expense of higher pressure drop across the domain. Figure 18, a multi-objective optimization plot for minimizing the volume per heat transferred and pumping power, represents this conclusion as the flat plate has a good ratio between volume and heat exchanged at lower pumping power but with increasing pump power the increase in the ratio stalls while the TPMS continue to increase and surpass the flat plates with the exception of SP. The plot on Figure 18 also features an area where the all of the geometries analysed converge, with exception of SP. This area ($0.02 < \Delta P\dot{V}/L^3 < 0.06\ W/m^3$) represents the point where increased heat exchanger compactness implies increased pump power and TPMS are the better choice and decreased pump power means a less compact heat exchanger and the flat plate is the obvious choice.

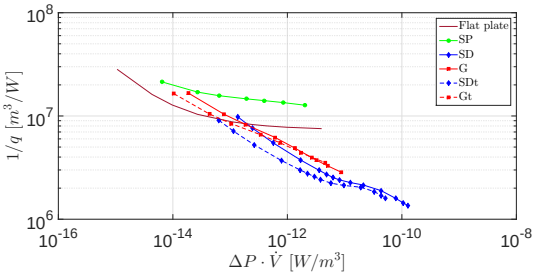

Figure 18: Heat exchanged vs inverse of pumping power.

To manufacture a heat exchanger, from the results presented here in this work, SDt presents it self as the best geometry due to higher convection properties allied with lower pressure drop and lower wall material used, in comparison with the SD.

5. Conclusions

The use of Triply Periodic Minimal surfaces (Schwarz-P, Schwarz-D and Schoen-Gyroid) on counter-flow heat exchangers was numerically investigated. For this, it was calculated pressure drop and heat transfer in the laminar steady regime across a representative elementary volume according to two energy models used in the literature for porous media. All the calculations were performed on a REV with periodic boundaries on Star-CCM+®. To the author's knowledge there are not many works studying heat transfer in porous media modelled as the Triply Periodic Minimal Surfaces.

The calculations of k_{eff} agree with the results found in the literature and show superior properties compared with anisotropic foams. The transition points to the unsteady laminar regimes based on the Re number were found. Two of the surfaces (Schwarz-P and Schoen-Gyroid) presented transition at $Re = 75$, lower than the values found in the literature. Schwarz-D topology presented transition at $Re = 150$ in accordance with the literature. From the Schwarz-D flow analysis, it was found the existence of three sub-regimes in the moderate Forchheimer regime, mixing, laminar transitional and inertial sub-regimes, that depend on the porosity and in the laminar transitional sub-regime there is a decrease in convection compared with the other two sub-regimes. Pressure drops were fitted to the Darcy-Forchheimer law based on the least-square method, and afterwards, values for permeability and form-drag coefficients were obtained.

Schwarz-P presented the lowest pressure drop and highest permeability values due to lower effective contact between the preferred stream and the wall. The pressure drop was made dimensionless through the friction factor and compared with the flat plate, noting that all the surfaces present exponential decay. TPMS have higher values compared with the flat plate and the porosity was found to have no influence on friction factor. Regarding convection two definitions of the Nu number for constant wall temperature, based on hydraulic diameter or periodic length, were evaluated and compared with the benchmark case. The Nu number based on the periodic length was found to be more useful to compare convection as it better reflects the behaviour of convection coefficient for periodic elements with the same REV size. Schwarz-D topology presented the highest values of convection coefficients followed by Schoen-Gyroid, the flat plate and Schwarz-P and the same tendency can be found in effectiveness. It was also found that convection coefficient inversely varies with the porosity. Wall material was related to the heat transferred across the wall and Schwarz-D presented the higher heat power per solid volume but increasing wall thickness this value compares to the Schoen-Gyroid with for same wall thickness but lower material used creating a threshold where for lower material usage the Schwarz-D is better and for higher material quantity Schoen-Gyroid is better. The increase in thermal performance calculated for Schwarz-D and Schoen-Gyroid is made at the expense of increased tortuosity and pump power. The flat plate was found to be the best solution at lower mass fluxes as it presents lower pump power and for higher heat transfer rates Schwarz-D and Schoen-Gyroid are better, making them suitable candidates for compact geometries.

References

[1] D. W. Abueidda, M. Bakir, R. K. Abu Al-Rub, J. S. Bergström, N. A. Sobh, and I. Jasiuk. Mechanical properties of 3D printed polymeric cellular materials with triply periodic minimal surface architectures. *Materials & Design*, 122:255–267, 2017.

[2] D. W. Abueidda, A. S. Dalaq, R. K. Abu Al-Rub, and H. A. Younes. Finite element predictions of effective multifunctional properties of interpenetrating phase composites with novel triply periodic solid shell architectured reinforcements. *International Journal of Mechanical Sciences*, 92:80–89, 2015.

[3] A. Dybbs and R. V. Edwards. *A New Look at Porous Media Fluid Mechanics — Darcy to Turbulent*. Springer Netherlands, Dordrecht, 1984.

[4] C. Fee. ScienceDirect 3D-printed porous bed structures. *Current Opinion in Chemical Engineering*, 18:10–15, 2017.

[5] T. Femmer, A. J. Kuehne, and M. Wessling. Estimation of the structure dependent performance of 3-D rapid prototyped membranes. *Chemical Engineering Journal*, 273:438–445, 2015.

[6] J. K. Guest and J. H. Prévost. Design of maximum permeability material structures. *Computer Methods in Applied Mechanics and Engineering*, 196(4-6):1006–1017, 2007.

[7] F. P. Incropera, A. S. Lavine, T. L. Bergman, and D. P. DeWitt. *Fundamentals of heat and mass transfer*. John Wiley & Sons, USA, 2007.

[8] Y. Jung and S. Torquato. Fluid permeabilities of triply periodic minimal surfaces. *Physical Review E - Statistical, Nonlinear, and Soft Matter Physics*, 72(5):1–8, 2005.

[9] F. Kuwahara, A. Nakayama, and H. Koyama. A numerical study of thermal dispersion in porous media. *Journal of Heat Transfer*, 118(3):756, 1996.

[10] F. Kuwahara, M. Shirota, and A. Nakayama. A numerical study of interfacial convective heat transfer coefficient in two-energy equation model of porous media. *International Journal of Heat and Mass Transfer*, 44(6):1153–1159, 2001.

[11] S. Mahjoob and K. Vafai. A synthesis of fluid and thermal transport models for metal foam heat exchangers. *International Journal of Heat and Mass Transfer*, 51(15-16):3701–3711, 2008.

[12] M. A. Mendes, S. Ray, and D. Trimis. A simple and efficient method for the evaluation of effective thermal conductivity of open-cell foam-like structures. *International Journal of Heat and Mass Transfer*, 66:412–422, 2013.

[13] R. K. Shah and A. L. London. *Laminar flow forced convection heat transfer and flow friction in straight and curved ducts*. Academic Press, 1978.

[14] N. Sreedhar, N. Thomas, O. Al-Ketan, R. Rowshan, H. H. Hernandez, R. K. Abu Al-Rub, and H. A. Arafat. Mass transfer analysis of ultrafiltration using spacers based on triply periodic minimal surfaces: Effects of spacer design, directionality and voidage. *Journal of Membrane Science*, 561:89–98, 2018.

[15] S. Whitaker. *Theory and Applications of Transport in Porous Media: The method of volume averaging*, volume 13. Springer Science & Business Media, Israel, 1999.

[16] C. Y. Zhao. Review on thermal transport in high porosity cellular metal foams with open cells. *Heat and Mass Transfer*, 55(13-14):3618–3632, 2012.